Proceedings of the ASME 2023
International Design Engineering Technical Conference and
Computers and Information in Engineering Conference
IDETC/CIE2023
August 20–23, 2023, Boston, Massachusetts

DETC2023-116752

NUMERICAL OPTIMIZATION OF UNDERACTUATED FLEXURE-BASED GRIPPERS

Boi Okken[1,3,*], Jan P. Dekker[2], Jan J. de Jong[1], Dannis M. Brouwer[1]

[1]Chair of Precision Engineering, University of Twente, Enschede, Netherlands
[2]Work performed whilst with the Chair of Precision Engineering, University of Twente[1]
[3]Robotics and Mechatronics Group, University of Twente, Enschede, Netherlands

ABSTRACT

Robotic manipulation in the agri-food industry faces several issues, including object variation, fragility and food safety. Underactuated flexure-based gripper allow passive adaptation to object variation, whilst monolithic flexure joints drive down cost, part-count, hygiene requirements, contamination and wear. However, designing flexure-based grippers presents challenges in achieving sufficient support stiffness, load-bearing capacity and joint deflection. Additionally, modeling the non-linear flexure behavior may become computationally expensive, especially under wide a variety of load cases, limiting the optimization approaches to simple structures and joints. In this work we present an interleaved computational optimization algorithm for underactuated flexure-based grippers, aimed at maximizing the range of graspable circular objects under a given load. This method achieves a superior design faster than state-of-the-art methods that optimize all design parameters simultaneously. A prototype constructed using rapid-prototyping validates the usage of the design method, and experimentally illustrates gripper performance.

Keywords: Grasping, Gripping, Compliant mechanism, Flexures, Optimization, Flexure-hinges, Under-actuation

FIGURE 1: DEVELOPED PHYSICAL PROTOTYPE WITH APPLE.

1. INTRODUCTION

The application of robotics in the agri-food industry is ripe with challenges [1–3]. High throughput is required to make robotising viable, whilst a cluttered and unstructured environment brings its own set of problems to deal with. Unique to the agri-food field are that hygiene and food-safety are of importance. All of these problems extend to the design of robotic grippers [4].

The uncertainty due to the environment, variation in size and fragility of objects implies that adaptability is desired. Employing passive compliance is one of the ways of improving gripper adaptability, as is done by 'soft' grippers [5–7]. Examples include fin-ray effect grippers [8, 9] , soft tentacles [10–12] and compliant surfaces. Although providing shape adaptability, the high compliance may also limit grasp determinism and stability under external loads.

A different way to tackle the adaptation problem is by way of intentional non-actuated degrees of freedom in pin-jointed gripper mechanisms [13–18]. Here the gripper adapts to the object shape through the underactuated nature of the mechanism rather than the inherent limited compliance of the material used in gripper construction. This kinematic adaptation relies on linkage mechanisms with hinges, which may be associated with decreased cost-effectiveness, reliability, and hygiene.

*Corresponding author: b.okken at utwente.nl

To cope with the aforementioned drawbacks, the underactuated gripper presented in this paper makes use of flexural bearings. Flexure-based joints provide unique solutions to the previously mentioned problems in agri-food gripping. In particular, due to the lack of lubrication or moving interfaces between parts, flexure-based grippers exhibit a increased reliability and food safety. However, flexures are inherently limited in stroke, loadability, and are typically harder to design for. Their inherent non-linear behaviour requires high-fidelity models which can be computationally expensive, especially when applied to grippers with a large amount of hinges, loading scenarios and object variation. Most existing literature therefore sticks to relatively simple flexure joints such as single blade flexures [19–22]. More complex joint structures provide additional avenues for design improvements [23], such as increase stiffness, stroke or load-bearing capabilities. As the complexity of the joints increases, the number of design parameters and thus gripper design space increases exponentially. Additionally, parameters arising from task complexity, such as complex loading conditions, types of grasp and applied actuator force, further exacerbates the previously mentioned problem of modeling and optimization, whether using analytical or computational approaches.

This paper presents a numerical optimization approach to design underactuated flexure-based grippers with stable 5-point grasp. The method is able to deal with complex flexure joints, geometries and loading scenarios.

The main contributions are as follows:

- A computational optimization-based design method of planar, underactuated grippers using flexure-joints, with the aim of maximizing the range of circular objects.
- An analytical method to compute worst case loading when grasping a circular object under an external load of a given magnitude, reducing the number of possible loading scenarios.
- An interleaved method for optimisation, increasing the efficiency by splitting the process into two alternating optimisation steps;
- Experimental validation of the designed gripper, with a proposed gripper performance indicator based on loss of 5-point stable grasp.
- And a validation of the used model by using comparing eigenfrequencies.

The paper starts with an overview of the gripper (Section 2.1), briefly discussing its parameters how it achieves under-actuation. Also discussed are assumptions and simplifications made for the design of the optimization. This is followed by a presentation of the structure of the optimization method in Section 2.2. Due to its importance in achieving good performance, the parametric model used for evaluating a set of gripper parameters is separately discussed in the following Section 2.3. The optimization procedure has been used to design a proof-of-concept prototype. This prototype, together with a description of practical experiments and measurement setup, is discussed in Section 2.4. Then, the results of optimization performance and physical measurements are presented under Section 3.1 and Section 3.2 respectively. These results are subsequently discussed in Section 4. Finally the work is concluded (Section 6) and possibly interesting future venues identified in Section 5.

2. METHOD

2.1 Gripper architecture

The gripper consists of two planar, symmetric fingers. Each finger (Illustrated in Fig. 2) consists of two phalanges attached to the base and a 5-bar underactuated driving mechanism, which distributes the actuator force to the contact points. This is chosen over alternatives such as tendon based actuation to avoid excessive compression forces in finger hinges, as well as improving cleanability. Not shown is the actuated prismatic joint that applies a vertical force between link L_{11} and the base, link L_1.

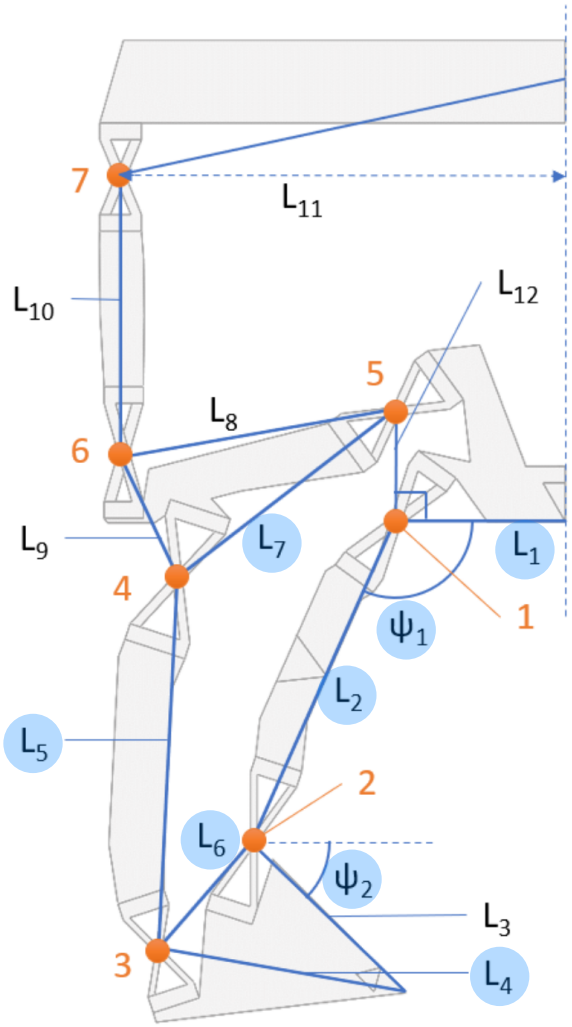

FIGURE 2: AN OVERVIEW OF A SINGLE FINGER OF THE FLEXURE-BASED GRIPPER, INCLUDING LABELS OF PRINCIPAL DIMENSIONS. BLUE LINES SIGNIFY RIGID BODIES, ORANGE DOTS REPRESENT THE HINGES.

To make computational optimization feasible with the complex joints, the task dimensionality is reduced by making the following assumptions. Firstly, we only consider symmetrical, circularly shaped objects. This restriction can be justified as many objects in the agri-food industry can be approximated with a circular cross-section. Secondly, we assume power grasp in which all phalanges and the palm make contact with the object such that gripper is form-closed, also fully defining its underactuated geometry. Thirdly, in order not to deviate from the circular shape assumption, a high stiffness of the object is presumed. Finally, a given maximum load on the object is assumed, of an unknown direction. The actuator force is chosen such to ensure stable 5-point contact under the given external load. Later, we will present the required conditions on the actuator and external force. The required conditions on actuator and external force are presented under Section 2.3.3.

The optimization method makes use of a full model, and in order to increase optimization speed, a pseudo-rigid model. It is assumed that flexure gripper's performance can be adequately approximated by this model, by neglecting pivot shift and load dependencies of the flexure hinges.

2.2 Optimization method

A schematic view of the proposed optimization method is shown in Fig. 3. A parametric model is used to evaluate the performance of the selected parameters, as this is more efficient than evaluating the full model. Because of its complexity this is discussed separately in Section 2.3.

The objective of the optimization is to maximize the range of objects that can be held in 5-point stable grasp, around a specified target radius, under a given load. The calculations responsible for the function evaluations are done within the parametric model, and hence are discussed further under Section 2.3.3.

2.2.1 Parameters and constraints. The gripper parameters are split into geometric and hinge parameters. These are elaborated upon further under Section 2.3.1 and 2.3.2 respectively.

The design space of the mechanism is bound by a chosen geometry. Some lengths of the mechanism are individually constrained to avoid interference. Table 1 shows a full list of geometric constraints, split into hinge geometry constraints (top) and gripper geometry constraints (bottom).

TABLE 1: CONSTRAINTS ON THE OPTIMIZATION. TOP HINGE GEOMETRY x_h, BOTTOM GRIPPER GEOMETRY x_g.

Parameter	Range
Hinge height h [mm]	0 - 20
Flexure thickness t [mm]	0 - ∞
Hinge width d [mm]	0 - ∞
Hinge tilt ϕ [deg]	0 - 360
Flexure angle θ [deg]	10 - 80
Element length L_i [mm]	0 - ∞
Neutral config. angle ψ_1 [deg]	90 - 180
Neutral config. angle ψ_2 [deg]	0 - 90

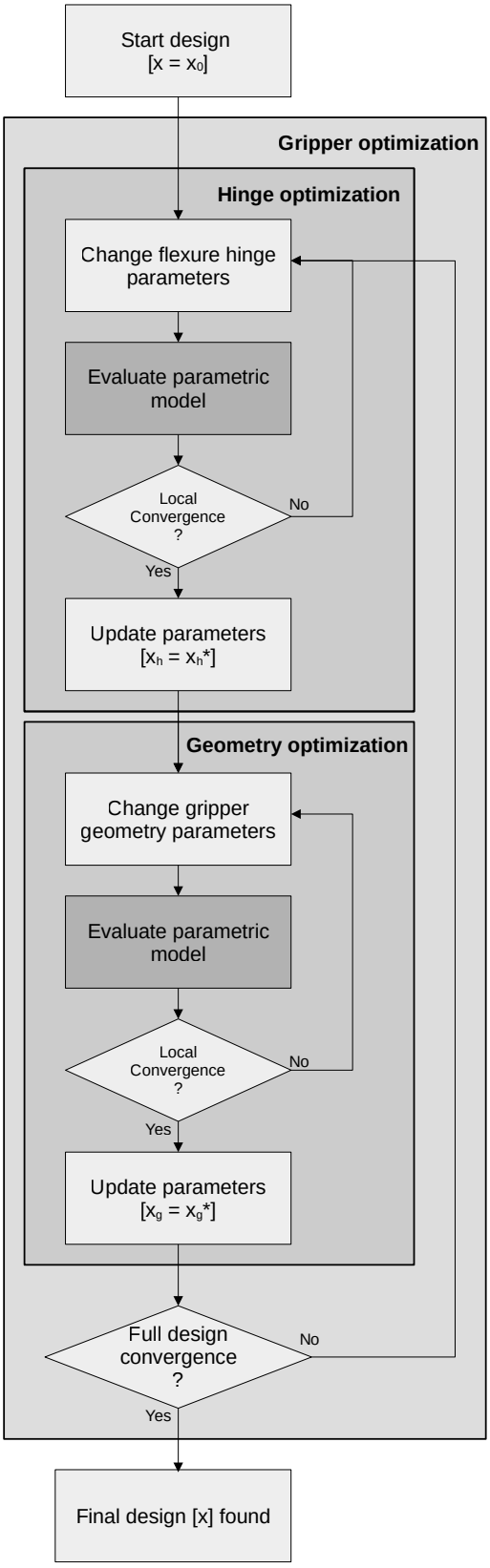

FIGURE 3: BLOCK DIAGRAM VIEW OF THE OPTIMIZATION METHOD. INTERNAL STRUCTURE OF THE PARAMETRIC MODEL IS SHOWN IN FIG. 4

2.2.2 Interleaved optimization method. The presented alternating optimization method works on the basis of an interleaved algorithm. It toggles between the optimization of hinge parameters (Section 2.3.2) and gripper geometry (Section 2.3.1) until a satisfying design is found. By treating hinge and gripper geometry optimization as separate problems the amount of parameters for each optimization are reduced, which significantly reduces the design space and thus computational load. However, the hinges and gripper geometry are not fully decoupled, and hence the interleaving provides an iterative way of finding a good design.

2.3 Parametric model

To evaluate a given load-case and radius, we want to ensure 5-point stable grasp (no loss of contact), no excessive stress, and no flexural buckling of the mechanism. A full model of the gripper could be used to establish performance of a set of chosen design parameters. However, doing so would be computationally expensive and hence not feasible to use for optimization. This is because besides object radius and external load, we also need to consider that the actuator provides sufficient force to obtain a stable equilibrium. This optimization problem might imply that for each function evaluation variations in radius, external force and actuator force are desired, leading to three dimensional evaluation. The simplified Pseudo-rigid finger model (PRBM) estimates the minimal required actuator effort to withstand the external force in any direction for a given radius. In order to avoid having to run n^3 simulation steps, the PRBM model is used to estimate the the minimal required actuator force to withstand external force for a given radius, ensuring 5-point stable grasp.

Hence the need of a parametric model, indicated in Fig. 3 as a dark colored box. This section goes into more detail in the implementation of this parametric model. A block diagram view of the parametric model is shown in Fig. 4.

2.3.1 Geometrical parameters. The geometry optimization adjusts a set of lengths of links in the finger. This set of parameters that are to be optimized are highlighted in light blue in Fig. 2. This leaves the non-optimized parameters L_3, L_8, L_9, L_{10}, L_{11} and L_{12}. L_9 and L_{12} are fixed to prevent hinge interference. L_8, L_{10} and L_{11}, if left unconstrained, would grow unbounded to minimize hinge deflections. Because of this these length are fixed or dependent on other parameters ($L_8 = L_7$, $L_{11} = L_1 + L_7$, $L_{10} = 50$ mm). Lastly, L_3 does not directly affect the optimization, but should be longer than the distance of hinge 2 to the contact point of the distal phalanx. Thus it is set with a length of 1.2x the distance between hinge 2 and the contact point, which is approximately $L_3 \approx 1.2L_1$. Note that additionally L_1 and L_{11} are fixed to be horizontal in the illustrated frame, whilst L_{12} is vertically oriented.

2.3.2 Hinge parameters. The hinge optimization addresses the parameters that define the shape of each flexure hinge. The hinge type chosen for demonstration of the proposed method is the triple flexure cross hinge (TFCH). This type is chosen due to its inherent high support stiffness over large deflection angles. It requires relatively little parameters to fully define, and thus is well suited for computational optimization. Additionally, symmetry

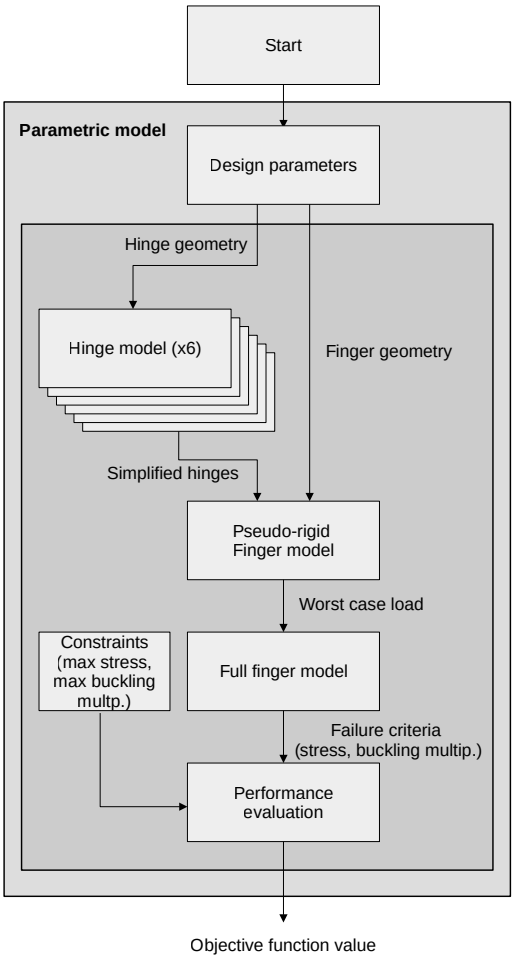

FIGURE 4: BLOCK DIAGRAM VIEW OF THE PARAMETRIC MODEL USED FOR DESIGN EVALUATION.

of the TFCH joint implies a high torsional stiffness compared to a cross pivot joint with two flexures. Lastly, the geometry is well suited to additive manufacturing methods.

The chosen triple cross flexure hinge is fully defined by a total of 5 parameters per joint, which are shown in Fig. 5. Every individual flexure that makes up the hinge has a given height h and thickness t. The individual flexures within the joint are distributed over width d such that the outer flexures have the same width as that of the inner flexure, with a gap existing between flexural elements of distance 0.05d in order to prevent interference. Finally angle θ determines the angle in the flexure joint, and the stiffness anistropy while angle ϕ indicates the stiffest direction orientation of the flexure relative the global gripper coordinate frame.

These parameters are used to generate a SPACAR model (Hinge model (x6) block in Fig. 4). This model is used to estimate the rotational actuation stiffness of each flexure hinge. This actuation stiffness estimation is subsequently used in the pseudo-rigid finger model to compute the required actuator force for stable 5-point contact.

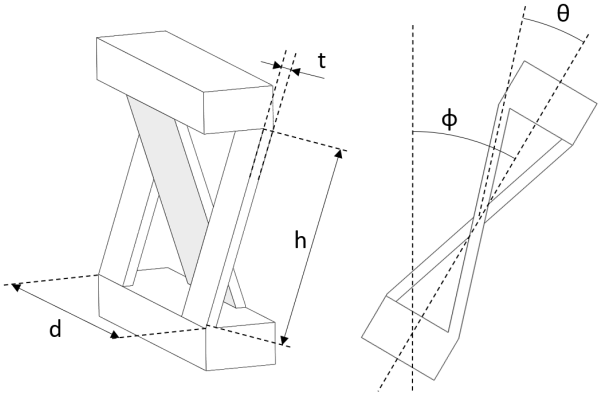

FIGURE 5: OVERVIEW AND PARAMETERS OF A SINGE TRIPLE CROSS FLEXURE JOINT.

2.3.3 Performance evaluation. The performance of each design is evaluated on a single worst load case for each object radius. The fully flexure-based finger is brought in contact with a circle of varying radius, whilst a sufficiently high actuator force is applied such that all contact forces remain positive. This condition is satisfied under any arbitrary direction of the external force of a given magnitude $f_{\max}$. Hence the load case corresponds to the highest compressive finger force f_{f} that each finger will endure at L_{10}. As there are in total 5 contact points during grasp, there exist five conditions of contact loss and thus worst case finger loads. In this section we describe how we determine the worst load case of these 5 candidates.

The method works as follows: First of all, we inspect a single finger, which due to symmetry, is also representative for the opposing finger. This gives rise to 3 worst case load candidates. Subsequently we compute the required actuator force in order to maintain contact on the opposing finger. Lastly, from the known information we compute the worst case finger load for all three possible candidates.

Each contact point experiences a contact force $\overline{f}_i = f_i \overline{n}_i$ with direction $\overline{n}_i$ pointing towards the object. Here $i \in \{1, 2, 3\}$ correspond with the distal, proximal and palm contact points respectively. The contact force magnitude is given by:

$$f_i = f_{i,\mathrm{el}}(r) + g_i(r) f_{\mathrm{a}} + e_{i,\mathrm{x}}(r) f_{\mathrm{x}} + e_{i,\mathrm{y}}(r) f_{\mathrm{y}} \tag{1}$$

In this equation $f_{i,\mathrm{el}}$ signifies the contact forces at rest due to elastic stress, f_{a} the applied actuator force, and f_{x} and f_{y} the external forces acting upon the object in the horizontal and vertical directions, respectively. The geometric transfer functions $g_i(r)$, $e_{i,\mathrm{x}}(r)$ and $e_{i,\mathrm{y}}(r)$ map the actuator and external force to the contact force. Due to symmetry, the palm contact force is influenced by vertical force only such that $e_{3,\mathrm{x}} = 0$, $e_{3,\mathrm{y}} = 1$ and $e_{1,\mathrm{y}} = e_{2,\mathrm{y}} = 0$.

By setting $f_i = 0$ in Eq. 1, three candidates for the minimal required actuator load f_{a} can be found. These in turn determines the three candidates for the maximal finger load:

$$f_{\mathrm{f}} = 1/2 f_{\mathrm{a}} + h(r) f_{\mathrm{x}} \tag{2}$$

in which $h(r)$ is a geometric transfer that determines how left and right finger carry the horizontal load.

Finding the worst case finger load for each radius is a matter of finding the maximum of the above three described candidate conditions on f_{f}:

$$f_{\mathrm{worstcase}}(r) = 1/2 \max \left\{ \begin{matrix} (2h - \frac{e_{1,x}}{g_1}) f_{\max} - \frac{f_{1,\mathrm{el}}}{g_1} \\ (2h - \frac{e_{2,x}}{g_2}) f_{\max} - \frac{f_{2,\mathrm{el}}}{g_2} \\ \sqrt{4h^2 + \frac{1}{g_3^2}} f_{\max} - \frac{f_{3,\mathrm{el}}}{g_3} \end{matrix} \right\} \tag{3}$$

In order to construct all of the above geometric transfer functions for the radii of interest, the PRBM simulation is run once with, and once without actuator force. As the gripper pose is fully defined by the presumed 5-point contact, a linear interpolation on the actuator force is used to find the geometric transfer functions and the elastic forces. The pseudo-rigid finger model is constructed with a torsional stiffness at each joint, as estimated by the hinge model described previously.

Although the pseudo-rigid model is a fair simplification, it neglects phenomena that constrain maximum finger loading such as internal stresses and buckling of the flexures in the hinges. To account for these, the found worst case load from the pseudo-rigid model is used in the 'full' non-linear flexible finger model, deducing the buckling multipliers and maximum stress in the hinges. To further model a realistic loading condition, an additional out-of-plane loading of $f_{\mathrm{oop}} = \frac{|f_{\mathrm{worstcase}}|}{2}$ is applied, which reduces hinge load capacity.

The set of feasible radii that can successfully be grasped, $\{r_{\mathrm{feasible}}\}$, is determined by constraints on the internal hinge stress $\sigma_{\max}$ and load buckling multipliers $\lambda_{\min}$:

$$\begin{aligned} \{r_{\mathrm{feasible}}\} &= \{r_{\mathrm{feas},\sigma}\} \cup \{r_{\mathrm{feas},\lambda}\} \\ r &\in \{r_{\mathrm{feas},\sigma}\} \text{ if } \sigma(r) \leq \sigma_{\max} \\ r &\in \{r_{\mathrm{feas},\lambda}\} \text{ if } \lambda(r) \geq \lambda_{\min} \end{aligned} \tag{4}$$

This is graphically illustrated in Fig. 6. Note that additional constraints on feasible boundaries might be present.

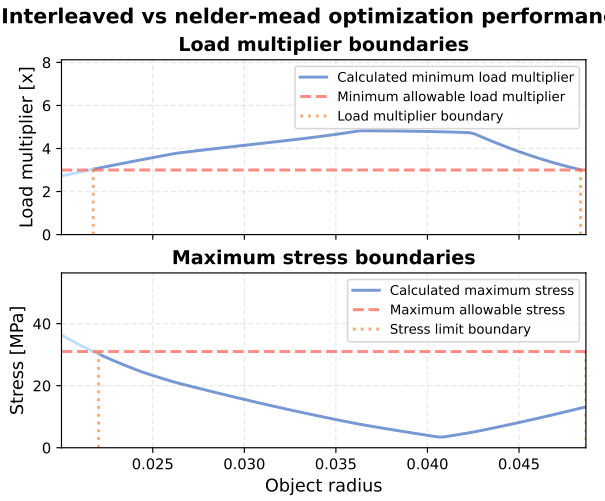

FIGURE 6: BOUNDARIES ON THE GRASPING RANGE, INDUCED BY MAXIMUM STRESS $\sigma_{\max}$ AND BUCKLING MULTIPLIER $\lambda_{\max}$.

Lastly, a score $\mathscr{F}$ is assigned to the evaluated design (Eq. 5). This score is proportional to the total gripping range around the targeted design radius r_{req}, which ensures that we maximize the gripping range. Note that this implies that the gripping range around the targeted design radius is not necessarily symmetrical.

$$\mathscr{F} = \frac{\min(r_{\text{feasible}})}{r_{\text{req}}} + \frac{r_{\text{req}}}{\max(r_{\text{feasible}})} \tag{5}$$

2.4 Proof-of-concept prototype

To demonstrate the effectiveness of the design method, a practical proof-of-concept prototype is designed and built (As shown in Fig. 1). The inherent ability for flexures to be monotonically manufactured increases cost-effectiveness and cleanability. SLS manufacturing is well suited for additive manufacturing, and is able to deal with a small minimum feature size. PA-12 Nylon is the material of choice for the prototype, as its high $\frac{\sigma_y}{E}$ compares favourably to other polymers (implying good flexural properties).

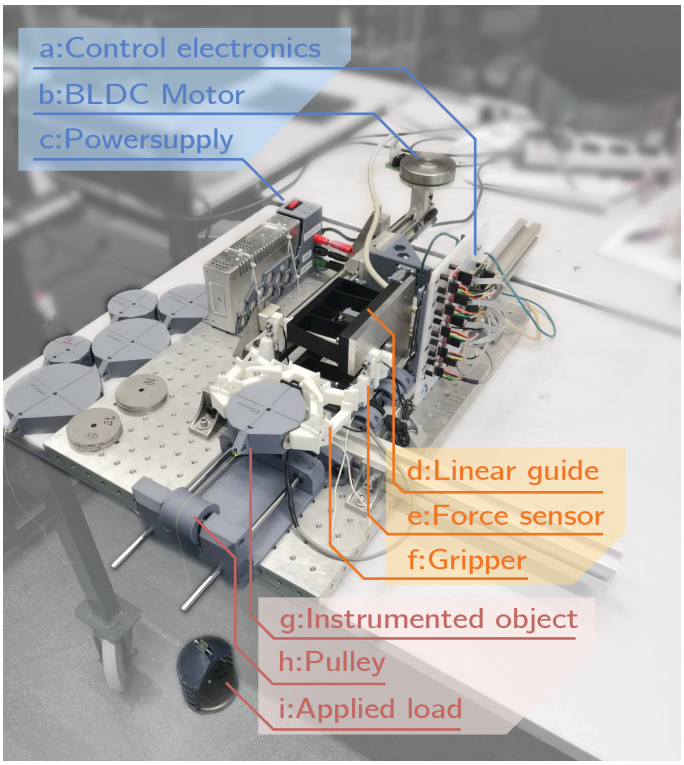

FIGURE 7: MEASUREMENT SETUP FOR PERFORMANCE EVALUATION.

2.4.1 Drive and support stiffness. To evaluate the model validity, drive and support stiffnesses of the practical prototype are compared to the model. Instead of measuring the stiffnesses directly, the systems resonant frequencies are measured using a high-speed camera and laser vibrometer. For these measurements the gripper is clamped at the base of the actuator, the actuator is fixed and an impulse is applied to the tip of the finger. These results are subsequently compared to the resonant frequencies of the numerical SPACAR model.

2.4.2 Gripper performance. To evaluate prototype gripper performance, instrumented objects of varying radii are placed in the gripper, and an external force is applied in the jaw opening direction. The contact forces at the expected locations are measured by loadcells embedded in the instrumented objects. Grip quality is thus measured by deducing the minimum required actuator force to maintain 5-point contact under a given external load. Note that loss of 5-point grasp does not imply grasp failure, as the gripper can reconfigure itself into a different stable configuration such as 4-point grasp[13].

A *Maxon Motor EC-90*[24] brushless DC motor is used in combination with a belt and pulley connected to a linear guide, generating the required linear force. This is fed through flexural couplings that guide the gripper. Load-cells integrated in the gripper structure measure the force applied to the gripper. Figure 7 shows the prototype in the measurement setup for gripper performance evaluation.

3. RESULTS

3.1 Optimization performance

To empirically illustrate the effectiveness of the proposed interleaved design algorithm, the number of function evaluations and score are measured. These are shown in Fig. 8.

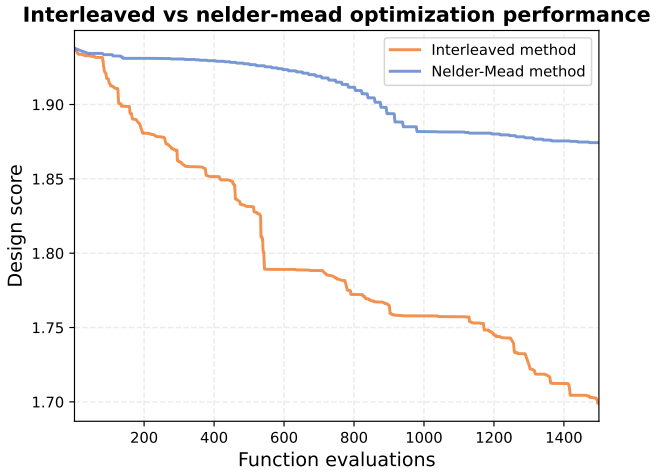

FIGURE 8: OPTIMIZATION PERFORMANCE COMPARISON OF A NELDER-MEAD BASED ALGORITHM AND THE PROPOSED INTERLEAVED OPTIMIZATION METHOD.

It can be seen that the proposed interleaved method reaches a lower function value for a similar amount of function evaluations. The lower final function value at convergence indicates a better design according to the selected optimization criteria.

A single function evaluation using a consumer *Intel Core i7-4700MQ* central processor unit, running at 2.40GHz is approximately 12 seconds. Total time for the illustrated optimization was approximately 5 hours.

The final design by the Nelder-Mead and interleaved optimization method result in a feasible radii range of $36.1-42.4$ mm and $32.9-45.8$ mm respectively. Thus in this example the interleaved method offers an increase in grasping range of 6.6 mm.

3.2 Prototype performance

3.2.1 Drive and support stiffness. The resonant frequencies of both the model and the developed prototype are shown in Table 2. For these experiments the actuator is fixed in place, and thus the lowest resonant frequency corresponds with the underactuated mode of the gripper. The subsequent higher modes correspond with the support directions.

TABLE 2: NATURAL FREQUENCIES OF MODEL AND PROTOTYPE.

Eigenfrequency #	Full model [Hz]	Prototype [Hz]
1	26.0	26.8
2	39.6	44.0
3	136	144
4	276	266

3.2.2 Gripper performance. The results of the gripper performance measurements are shown in Fig. 9. A point in the graph can be interpreted as the minimally required actuator force, to keep a circular object with given applied force in 5-point stable grasp.

Considering a line of a given radius object in Fig. 9, we can observe two distinct regions. Firstly a linear region, in which an increasing load requires a proportional increase in actuator force to sustain 5-point stable grasp. The slope is an indication of ability to transfer force of the gripper from actuator to the contact points. This slope is dependent on forces needed to deform the gripper (or elastic forces helping to keep the object in place), and location of the point of contact due to different force distribution from a given structure configuration. Thus this line can be used to deduce a given force-transfer characteristic of a specific configuration. The force generated by the palm can only be opposed by the vertical force component of the distal contact, and hence a larger gripper opening requires a substantially higher force to produce a given palm reaction force.

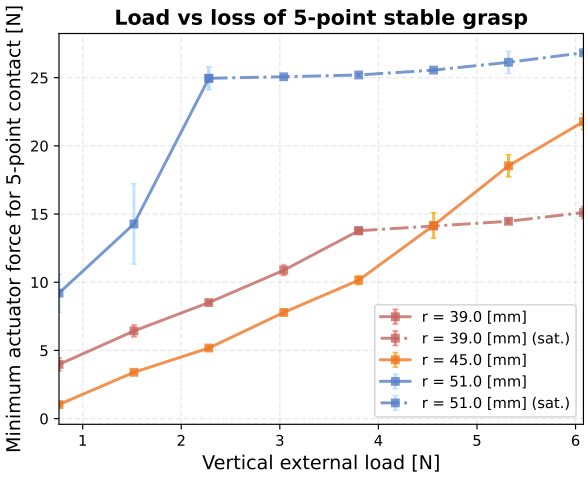

FIGURE 9: GRIPPER PERFORMANCE FOR DIFFERENT OBJECT RADII. DOTTED LINES IMPLY ACTUATOR SATURATION.

The linear region plateaus into the 'saturation' region, illustrated in Fig. 9 by the dotted lines. For the presented results this is a measurement artifact, caused by the actuator being limited in it maximum torque. Even when applying maximum torque there is no 5-point grasp. If a more powerful actuator would be used, we still expect a plateau region, where flexural buckling occurs due to excessive flexure loading, leading to loss of contact regardless of an increase in supplied actuator force. The different minimum actuator force of the different plateaus can be explained due to the change in gripper configuration, and elastic component contribution of the flexure joints. As explained previously these can result in a different force transfer from actuator to contact forces.

4. DISCUSSION

4.1 Optimization

What is not clear from the results of the optimization directly, are the following observations:

1. Hinge 1, 6 and 7 have high loads, and as a result are optimized to have high stiffness in drive and support directions;
2. Hinge 2 and 5 have high deformation, and as a result are optimized to have low stiffness;
3. All hinges are rotated such, that the load goes 'straight' through the joint (i.e. $\phi = \angle F_{\text{load}}$).

4.2 Prototype

The design found by the design method does not guarantee that the fingers are able to fully open to fit the largest size objects into grasp. This could result in a situation where the largest objects might not fit through the jaws of the gripper, and these thus need to be loaded by lowering the gripper onto them.

Additionally, the opening motion of the gripper is determined by the geometry configuration and elasticity of hinges. To address this issue, end-stops have been implemented.

As for the gripper performance, there exists an optimum where the elastic component and the distal contact angle balance, requiring the lowest amount of actuator force to hold an object in 5-point stable grasp. For the presented data this appears to be close to the $r = 45$ mm object size.

During experiments it was seen that larger radius objects are sensitive to alignment. A small rotation can cause a significant shift in observed actuator force required for 5-point contact with a given load.

5. FUTURE WORK

Changes to the interleaved optimization algorithm would allow extension to non-circular and non-uniform objects. Fruitful results here would further extent the capabilities of the gripper, particularly for real-world scenarios. Loss of 5-point grasp does not always result in grasp failure. Expanding the method to take into into account other grasp configurations, and analyzing their performance is an interesting avenue to further refine the existing design.

Some preliminary results of gripper performance have been illustrated. The usage of a more powerful actuator would allow the demonstration of the mechanical limitation of the designed gripper, as opposed to actuator limitations.

6. CONCLUSION

The application of robotic grippers in the agri-food industry has many unique challenges. In view of tackling these challenges, this work presents a design method for grippers, with a focus on handling a large variety of objects under external load. The design is able adapt through under-actuation, and the usage of flexure joints makes the design both cost effective and hygienic.

The proposed interleaved gripper design method for flexure-based, planar underactuated grippers successfully navigates a large design space, coming up with a superior solution, faster than non-interleaved computational optimization methods, whilst taking into account buckling and stress. It shows that flexure-based gripper design does not need to be limited to single blade flexure joints, and that more elaborate flexure joint designs can be used.

The 3D printed practical prototype out of SLS PA12 Nylon illustrates the effectiveness of the design method, designed for a range of objects from 32.9-45.8 mm radius, and showing a practically realizable grasping range of at least 39 to 51 mm. Design parameters show that this design is able to resist external loads of at least 5 N for any radius, in any direction of at least 5N. Part of the designed operating range regarding different radii objects and loads have been tested, showing promising real-world performance.

Experiments validate eigenfrequencies in drive and lowest support directions of the model, illustrating that the high fidelity model can approximate real world behavior.

DECLARATION OF CONFLICT OF INTEREST

The authors hereby declare that there were no possible conflicts of interest in the production of this work.

ACKNOWLEDGMENTS

The work presented has been done under the FlexCRAFT project, funded by NWO/TTW under grant *"P17-01 Flexcraft - P4 Gripping and manipulation"*.

REFERENCES

[1] Oliveira, Luiz F. P., Moreira, António P. and Silva, Manuel F. "Advances in Agriculture Robotics: A State-of-the-Art Review and Challenges Ahead." *Robotics* Vol. 10 No. 2 (2021). DOI 10.3390/robotics10020052. URL https://www.mdpi.com/2218-6581/10/2/52.

[2] Khan, Zeashan Hameed, Khalid, Azfar and Iqbal, Jamshed. "Towards realizing robotic potential in future intelligent food manufacturing systems." *Innovative Food Science & Emerging Technologies* Vol. 48 (2018): pp. 11–24. DOI https://doi.org/10.1016/j.ifset.2018.05.011. URL https://www.sciencedirect.com/science/article/pii/S1466856417300401.

[3] Duong, Linh N.K., Al-Fadhli, Mohammed, Jagtap, Sandeep, Bader, Farah, Martindale, Wayne, Swainson, Mark and Paoli, Andrea. "A review of robotics and autonomous systems in the food industry: From the supply chains perspective." *Trends in Food Science & Technology* Vol. 106 (2020): pp. 355–364. DOI https://doi.org/10.1016/j.tifs.2020.10.028. URL https://www.sciencedirect.com/science/article/pii/S0924224420306518.

[4] Vrochidou, Eleni, Tsakalidou, Viktoria Nikoleta, Kalathas, Ioannis, Gkrimpizis, Theodoros, Pachidis, Theodore and Kaburlasos, Vassilis G. "An Overview of End Effectors in Agricultural Robotic Harvesting Systems." *Agriculture* Vol. 12 No. 8 (2022). DOI 10.3390/agriculture12081240. URL https://www.mdpi.com/2077-0472/12/8/1240.

[5] Zhang, Ping and Tang, Bin. "A Two-Finger Soft Gripper Based on Bistable Mechanism." *IEEE Robotics and Automation Letters* Vol. 7 No. 4 (2022): pp. 11330–11337. DOI 10.1109/LRA.2022.3200207.

[6] Stabile, Christopher J., Levine, David J., Iyer, Gokulanand M., Majidi, Carmel and Turner, Kevin T. "The Role of Stiffness in Versatile Robotic Grasping." *IEEE Robotics and Automation Letters* Vol. 7 No. 2 (2022): pp. 4733–4740. DOI 10.1109/LRA.2022.3149036.

[7] Puente-Flores, Alfredo, Roman-Flores, Armando, Cuan-Urquizo, Enrique, Vazquez-Hurtado, Carlos and Urbina-Coronado, Pedro. "Design of a Single Actuated Soft Gripper with Compliant Mechanisms." *2022 10th International Conference on Control, Mechatronics and Automation (ICCMA)*: pp. 276–280. 2022. DOI 10.1109/ICCMA56665.2022.10011605.

[8] Elgeneidy, Khaled, Lightbody, Peter, Pearson, Simon and Neumann, Gerhard. "Characterising 3D-printed Soft Fin Ray Robotic Fingers with Layer Jamming Capability for Delicate Grasping." *2019 2nd IEEE International Conference on Soft Robotics (RoboSoft)*: pp. 143–148. 2019. DOI 10.1109/ROBOSOFT.2019.8722715.

[9] Yang, Yang, Jin, Kaixiang, Zhu, Honghui, Song, Gongfei, Lu, Haojian and Kang, Long. "A 3D-Printed Fin Ray Effect Inspired Soft Robotic Gripper with Force Feedback." *Micromachines* Vol. 12 No. 10 (2021). DOI 10.3390/mi12101141. URL https://www.mdpi.com/2072-666X/12/10/1141.

[10] Xie, Zhexin, Yuan, Feiyang, Liu, Zemin, Sun, Zhaoning, Knubben, Elias M. and Wen, Li. "A Proprioceptive Soft Tentacle Gripper Based on Crosswise Stretchable Sensors." *IEEE/ASME Transactions on Mechatronics* Vol. 25 No. 4 (2020): pp. 1841–1850. DOI 10.1109/TMECH.2020.2993258.

[11] G, Mageshkumar, S, Suthagar, N, Mukilarasu, K S, Nandesh, T, Lakshmikanthan and K S, Tamilselvan. "Design and Analysis of a Soft Gripper for Human Interactive Robot." *2022 6th International Conference on Computing Methodologies and Communication (ICCMC)*: pp. 563–568. 2022. DOI 10.1109/ICCMC53470.2022.9753818.

[12] Garcia Rubiales, F. Javier, Ramon Soria, Pablo, Arrue, Begoña C. and Ollero, Anibal. "Soft-Tentacle Gripper for Pipe Crawling to Inspect Industrial Facilities Using UAVs." *Sensors* Vol. 21 No. 12 (2021). DOI 10.3390/s21124142. URL https://www.mdpi.com/1424-8220/21/12/4142.

[13] Kragten, Gert and Herder, Just. "A planar geometric design approach for a large grasp range in underactu-

ated hands." *Mechanism and Machine Theory - MECH MACH THEOR* Vol. 46 (2011): pp. 1121–1136. DOI 10.1016/j.mechmachtheory.2011.03.004.

[14] Kragten, Gert, Baril, Mathieu, Gosselin, Clément and Herder, Just. "Stable Precision Grasps by Underactuated Grippers." *IEEE Transactions on Robotics* Vol. 27 (2011): pp. 1056–1066. DOI 10.1109/TRO.2011.2163432.

[15] Boisclair, Jean-Michel, Laliberte, Thierry and Gosselin, Clément. "On the Design of an Adaptable Underactuated Hand Using Rolling Contact Joints and an Articulated Palm." *Journal of Mechanisms and Robotics* Vol. 15 (2022): pp. 1–25. DOI 10.1115/1.4055605.

[16] Tamamoto, Takumi, Takeuchi, Keita and Koganezawa, K. "Development of Gripper to Achieve Envelope Grasping with Underactuated Mechanism Using Differential Gear." *Journal of Robotics and Mechatronics* Vol. 30 (2018): pp. 855–862. DOI 10.20965/jrm.2018.p0855.

[17] Borisov, Ivan I., Khomutov, Evgenii E., Kolyubin, Sergey A. and Stramigioli, Stefano. "Computational Design of Reconfigurable Underactuated Linkages for Adaptive Grippers." *2021 IEEE/RSJ International Conference on Intelligent Robots and Systems (IROS)*: pp. 6117–6123. 2021. DOI 10.1109/IROS51168.2021.9636792.

[18] Yan, Yonggan, Guo, Shuxiang, Yang, Cheng, Lyu, Chuqiao and Zhang, Liuqing. "The PG2 Gripper: an Underactuated Two-fingered Gripper for Planar Manipulation." *2022 IEEE International Conference on Mechatronics and Automation (ICMA)*: pp. 680–685. 2022. DOI 10.1109/ICMA54519.2022.9856375.

[19] Chang, Che-Ming, Gerez, Lucas, Elangovan, Nathan, Zisimatos, Agisilaos and Liarokapis, Minas. "On Alternative Uses of Structural Compliance for the Development of Adaptive Robot Grippers and Hands." *Frontiers in Neurorobotics* Vol. 13 (2019). DOI 10.3389/fnbot.2019.00091.

[20] Achilli, Gabriele Maria, Logozzo, Silvia, Valigi, Maria Cristina, Salvietti, Gionata, Prattichizzo, Domenico and Malvezzi, Monica. "Underactuated Soft Gripper for Helping Humans in Harmful Works." Quaglia, Giuseppe, Gasparetto, Alessandro, Petuya, Victor and Carbone, Giuseppe (eds.). *Proceedings of I4SDG Workshop 2021*: pp. 264–272. 2022. Springer International Publishing, Cham.

[21] Cammarata, Alessandro, Maddio, Pietro Davide, Sinatra, Rosario and Belfiore, Nicola Pio. "Direct Kinetostatic Analysis of a Gripper with Curved Flexures." *Micromachines* Vol. 13 No. 12 (2022). DOI 10.3390/mi13122172. URL https://www.mdpi.com/2072-666X/13/12/2172.

[22] Kuresangsai, Pongsiri, Cole, Matthew O. T. and Hao, Guangbo. "Grasp Stability and Design Analysis of a Flexure-Jointed Gripper Mechanism via Efficient Energy-Based Modeling." *IEEE Robotics and Automation Letters* Vol. 7 No. 4 (2022): pp. 12499–12506. DOI 10.1109/LRA.2022.3220152.

[23] Naves, M., Brouwer, D.M. and Aarts, R.G.K.M. "Building Block-Based Spatial Topology Synthesis Method for Large-Stroke Flexure Hinges." *Journal of Mechanisms and Robotics* Vol. 9 No. 4 (2017). DOI 10.1115/1.4036223. 041006.

[24] "Maxon EC 90 flat 90W, BLDC Motor datasheet." URL https://www.maxongroup.com/medias/sys_master/8825435389982.pdf.